Downloaded from orbit.dtu.dk on: Mar 27, 2025

DTU Library

In vitro recording of muscle activity induced by high intensity laser optogenetic stimulation using a diamond quantum biosensor

Troise, Luca; Hansen, Nikolaj Winther; Olsson, Christoffer; Webb, James Luke; Tomasevic, Leo; Achard, Jocelyn; Brinza, Ovidiu; Staacke, Robert; Kieschnick, Michael; Meijer, Jan

Total number of authors:
16

Published in:
AVS Quantum Science

Link to article, DOI:
10.1116/5.0106099

Publication date:
2022

Document Version
Peer reviewed version

Link back to DTU Orbit

Citation (APA):
Troise, L., Hansen, N. W., Olsson, C., Webb, J. L., Tomasevic, L., Achard, J., Brinza, O., Staacke, R., Kieschnick, M., Meijer, J., Thielscher, A., Siebner, H. R., Berg-Sørensen, K., Perrier, J. F., Huck, A., & Andersen, U. L. (2022). In vitro recording of muscle activity induced by high intensity laser optogenetic stimulation using a diamond quantum biosensor. *AVS Quantum Science*, *4*(4), Article 044402. https://doi.org/10.1116/5.0106099

General rights
Copyright and moral rights for the publications made accessible in the public portal are retained by the authors and/or other copyright owners and it is a condition of accessing publications that users recognise and abide by the legal requirements associated with these rights.

- Users may download and print one copy of any publication from the public portal for the purpose of private study or research.
- You may not further distribute the material or use it for any profit-making activity or commercial gain
- You may freely distribute the URL identifying the publication in the public portal

If you believe that this document breaches copyright please contact us providing details, and we will remove access to the work immediately and investigate your claim.

In-vitro recording of muscle activity induced by high intensity laser optogenetic stimulation using a diamond quantum biosensor

Luca Troise,[1, a)] Nikolaj Winther Hansen,[2, a)] Christoffer Olsson,[3, a)] James Luke Webb,[1, b)] Leo Tomasevic,[4] Jocelyn Achard,[5] Ovidiu Brinza,[5] Robert Staacke,[6] Michael Kieschnick,[6] Jan Meijer,[6] Axel Thielscher,[3] Hartwig Roman Siebner,[7, 8] Kirstine Berg-Sørensen,[3] Jean-François Perrier,[2] Alexander Huck,[1] and Ulrik Lund Andersen[1]

[1)]*Center for Macroscopic Quantum States (bigQ), Department of Physics, Technical University of Denmark, 2800 Kgs. Lyngby, Denmark*

[2)]*Department of Neuroscience, University of Copenhagen, Copenhagen, Denmark*

[3)]*Department of Health Technology, Technical University of Denmark, 2800 Kgs. Lyngby, Denmark*

[4)]*Danish Research Centre for Magnetic Resonance, Centre for Functional and Diagnostic Imaging and Research, Copenhagen University Hospital - Amager and Hvidovre, Kettegaard Alle 30, 2650 Hvidovre, Denmark*

[5)]*Laboratoire des Sciences des Procédés et des Matériaux, Université Sorbonne Paris Nord, 93430 Villetaneuse, France*

[6)]*Division Applied Quantum System, Felix Bloch Institute for Solid State Physics, Leipzig University, 04103, Leipzig, Germany*

[7)]*Department of Neurology, Copenhagen University Hospital Bispebjerg and Frederiksberg, Bispebjerg Bakke 23, 2400 Copenhagen, Denmark*

[8)]*Department of Clinical Medicine, Faculty of Health and Medical Sciences, University of Copenhagen, Blegdamsvej 3B, 2200 Copenhagen N, Denmark*

(*james.webb2@gmail.com, jaluwe@fysik.dtu.dk)

(Dated: 29 August 2022)

The detection of physiological activity at the microscopic level is key for understanding the function of biosystems and relating this to physical structure. Current sensing methods for *in vitro* study of living tissue often rely on invasive probes to stimulate and detect activity, bearing the risk of inducing damage in the target system. In recent years, a new type of quantum sensor based on color centers in diamond has begun to offer the possibility to instead passively sense and image living biological systems. Here, we use such a sensor to realize the recording of the biomagnetic field generated by tightly focused, high intensity pulsed laser optogenetic neuromuscular stimulation of extensor digitorum longus muscles, dissected from from mice and kept alive in carbogenated solution. Recordings captured a compound action potential response and a slow signal component which we seek to explain using a detailed model of the biological system. We show proof of principle experimental recording of localized neuromuscular activity from the laser stimulation site without photovoltaic or fluorescence artifacts associated with alternative techniques. Our work represents a further step towards passive sensing and imaging at the microscopic level with quantum sensing, enabling further research into mapping of neural activity and intra-cellular processes.

I. INTRODUCTION

Sensing biological activity at the microscopic level in a cell culture or tissue slice kept alive *in vitro* is of fundamental importance for understanding the basic processes in living organisms[1]. Relating activity, including electrical and thermal transport, to cell structure and are key steps to decipher biological functions in health and their alterations in disease, for example in the understanding of the early stages of neurodegenerative disorders. Of particular interest is the biological response to a stimulus, such as a pulse of electrical current or light, and being able to detect this response with high spatial and temporal resolution[2]. Many different sensing approaches have been developed for microscopic direct detection of activity, in particular recording of electrical activity using probe electrodes (electrophysiology), including multi-electrode arrays, and by sensing using fluorescent biomarkers under laser illumination[3,4]. However such methods, involving direct interaction with laser light or mechanical placement of sharp electrodes, can risk cell death or tissue damage through heating or mechanical action[5,6]. Furthermore, the data obtained may depend strongly on the quality of the measurement, in terms of variable electrical conductivity and contact in the case of electrical probes or the quantity of biomarkers expressed in a given cell or tissue for fluorescence microscopy leading to inaccuracy, especially where quantitative comparisons are required.

An alternative method is to indirectly detect activity, passively sensing from outside of the sample. For electrical activity, this can be achieved by monitoring the magnetic field induced by the signal, which can freely penetrate solutions and biological tissue in a way not possible by electrical potential or light. For whole organisms, field sensing has been demonstrated for low resolution sensing of electrical activity in the brain (magnetoencephalography,MEG) and the heart (magnetocardiography, MCG), using superconducting quantum interference device (SQUID) sensors[7,8]. However, these sensors have significant disadvantages, requiring

[a)]These authors contributed equally to this work

[b)]These authors contributed equally to this work; Main corresponding author

PLEASE CITE THIS ARTICLE AS DOI: 10.1116/5.0106099

special shielding from background magnetic field (e.g. geomagnetic, mains electricity) and cryogenic cooling, limiting these valuable techniques to very few facilities and applications and constraining the spatial resolution they can achieve to the macro/mesoscale only.

In recent years, new approaches without these drawbacks have been actively sought[9–12]. Here, quantum technology offers a potential solution. In this work, we focus on an approach to biosensing utilizing quantum sensing based on color centers, atomic-scale defect sites in a solid state material with optical properties highly sensitive to their physical parameters and local environment. In particular, we focused on the use of negatively charged nitrogen vacancy (NV) centers in diamond, consisting of a nitrogen subsitutional dopant paired with a lattice vacancy. NV centers have been used for sensing of magnetic field[13], electric field[14], temperature[15] and strain (pressure/force)[16] via optically detected magnetic resonance (ODMR) spectroscopy[17,18]. Diamond NV sensing offers advantages including high sensitivity[19–21], room temperature operation and high spatial[22,23] and temporal[24] resolution. Diamond is highly biocompatible, enabling NV sensing to work in solution across a wide range of temperatures and pH values[25,26]. Such sensing can be performed remotely at a distance or in close contact (and even within) a biological specimen[27,28].

NV centers in diamond are particularly suited to microscopy applications in either widefield or confocal configurations[23,29,30], particularly for sensing from a small volume region, containing single (neuron) cells and down to the few or single molecule level, with spatial resolution which SQUIDs or other alternative techniques cannot reach. A desirable goal is to selectively and precisely optically stimulate activity while recording activity in a volume close to or at the site of stimulation, without suffering from the measurement artifacts that pose challenges for existing recording methods[31–33]. Achieving this goal is key to realizing applications including nanoscale nuclear magnetic resonance[34], radical pair sensing for avian magnetoreception[35], intracellular nanodiamond studies[26,36–38] and stimulation of neurons in brain tissue[39–41]. Due to the confinement required, focused laser stimulation is preferable for these applications, with the higher laser optical intensity ideal for for stimulation well within tissue.

In this work, we seek to perform a proof of principle study to demonstrate the viability of such focused laser stimulation combined with simultaneous microscopic quantum sensing from biological tissue located in proximity to the stimulation site. We use living *extensor digitorum longus* (EDL) muscles from mice *in vitro*, genetically modified to contain the light gated cation channel channelrhodopsin (ChR2)[42]. We stimulate the muscle tissue using focused pulsed laser light, of a specific wavelength and intensity, generating highly localized ($\approx$150μm) stimulation and activation of the muscle response. We then record the response of the muscle using NV sensing to detect the magnetic field induced by ionic current associated with compound action potentials in the muscle. We demonstrate highly focused stimulation with artifact-free recording of activity using NV centers with high temporal resolution and explore the biological response recorded under laser stimulation to derive new insight into the behavior of the biological system and response. To achieve this, we employ new methodology including spectral whitening filtering of background noise to enhance biosignal magnetic field recovery in an ordinary lab environment without magnetic shielding.

II. MATERIAL AND METHODS

A. Diamond NV Sensor

We used a [100] oriented electronic-grade diamond (Element Six), of dimensions $2 \times 2 \times 0.5$ mm^3, overgrown via chemical vapor deposition (CVD) with a 20μm thick diamond layer with a doping concentration of $\approx$5 ppm of ^{14}N. NV centers were generated by 2.8MeV proton irradiation and subsequent annealing at 800C. We measured an ODMR resonance linewidth of 1 MHz and a resonance contrast of 1.5% (see Supplementary Information for spectrum). The diamond was mounted into an aluminum nitride plate heatsink, with the top surface of the diamond covered by a 16μm thick layer of aluminum foil, reflecting pump laser back into the diamond and blocking the stimulation laser light from the diamond (Figure 1). The aluminum foil was covered by Kapton tape (50μm) to electrically insulate the diamond from the biological sample. The AlN plate holding the diamond was mounted on a printed board microwave antenna. On top of the diamond, we mounted a 3D printed plastic chamber for holding a solution bath, sealed using aquarium silicone.

B. Sensing Method

We optically pumped our diamond with 1.4W of 532nm green laser light (Coherent Verdi G2), linearly polarized and coupled to the diamond from beneath at Brewster's angle (67). The pump laser is entirely confined to the diamond and at no stage contacts the biological tissue under study. Red fluorescence from the NV centers was collected using a 12mm diameter condenser lens (Thorlabs ACL 1210) via an optical filter (FEL0600). Magnetic field at the diamond was recorded as a modulation of the intensity of the red fluorescence emission recorded using an auto-balanced optical receiver (Nirvana 2007, New Focus Inc.). We measured only the magnetic field response in the direction perpendicular to the electrical current propagation direction inside the muscle, with this single axis response maximized by applying a static bias field of 1.5 mT parallel to the diamond [110] crystallographic direction. A continuous wave scheme was implemented with three-frequency microwave driving scheme[43] using two microwave generators (Stanford SG394) to drive the triplet ground state transition (2.7-3GHz) and the ^{14}N hyperfine transitions (2.16 MHz). We applied microwave power of a maximum $\approx$15dBm before mixer and cable losses (up to 8dB and 2dB respectively), giving $\approx$45dBm after amplification (40 dB). The two RF signals were delivered to the diamond via a printed circuit board nearfield antenna, of design outlined in the work by

PLEASE CITE THIS ARTICLE AS DOI: 10.1116/5.0106099

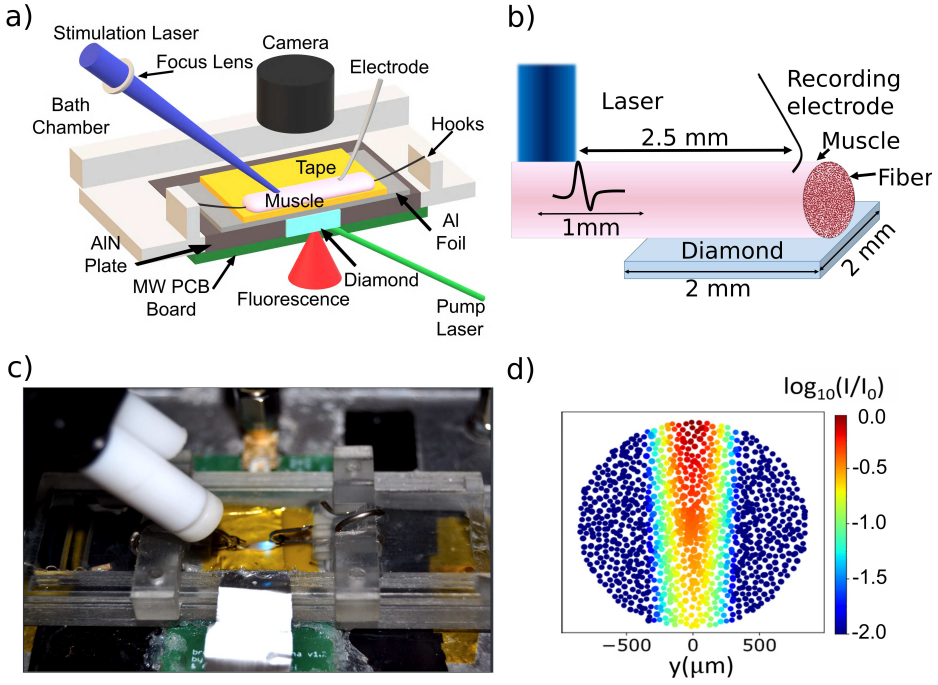

FIG. 1. **Experimental apparatus and muscle cross section** a) Schematic of the experimental setup and b) picture of the muscle in the solution chamber with a 488nm blue stimulation laser spot incident on the muscle surface. The laser spot could be placed with high precision anywhere within the sample chamber in a 2x2cm area using mechanical mirror mounts. c) Schematic illustration of experimental setup, as used in the modeling. d) Simulated cross-section of muscle showing the light intensity (I/I_0) distribution on the muscle fibers with laser stimulation.

Sasaki et al[44]. The microwaves were modulated at 23.3 kHz for lock-in detection (Stanford SR850), using a time constant of 30μs giving a measurement bandwidth of 4.8kHz. The output of the lock-in amplifier was digitized at 80 kSa/s using an analog to digital converter (NI PCI-6221) and recorded using custom-written software. In order to maintain maximum field sensitivity and compensate for any drift in resonance frequency due to slow temperature changes, an automated algorithm written in Labview was set to perform a series of ODMR spectra every 5 minutes, in order to set the microwave frequency and power to that corresponding to the point of maximum ODMR slope (point of maximum sensitivity).

C. Muscle Preparation

We used mice expressing the light sensitive cation channel Channelrhodopsin2 (ChR2) in muscle cells expressing Parvalbumin (PV) by crossing Gt(ROSA)26Sor$^{tm32(CAG-COP4*H134R/EYFP)Hze}$ (stock no.: 024109; Jackson Laboratory) mice with Pvalb$^{tm1(cre)Arbr}$ mice (stock no.: 017320; Jackson Laboratory)[42]. Adult PV-Cre::ChR2 mice were dissected as described previously[42]. Quickly following euthanasia by cervical dislocation, EDL muscles were dissected in carbogen (95% O_2/5% CO_2) saturated ice-cold artificial cerebrospinal fluid (ACSF) containing (in mM): NaCl (111), $NaHCO_3$ (25), glucose (11), KCl (3), $CaCl_2$ (2.5), $MgCl_2$ (1.3) and KH_2PO_4 (1.1). Small suture loops were tied on proximal and distal tendons. The dissected mouse muscle was kept in a solution bath of artificial cerebrospinal fluid (ACSF), chilled by passing a recycled feed of ACSF into the solution chamber through tubing submerged in ice to maintain a bath temperature between 18C and 20C. The ACSF was bubbled with carbogen gas to oxygenate the muscle and allow survival for up to 20 hours of measurement.

D. Laser Stimulation and Recording

The muscle was positioned on the diamond by two adjustable hooks and a probe electrode (AgCl coated silver wire) mounted on a micromanipulator placed in contact with the

PLEASE CITE THIS ARTICLE AS DOI: 10.1116/5.0106099

muscle top surface. The electric data from this probe electrode was recorded via a differential amplifier (Axon Cyberamp 320) relative to the grounded solution bath. Muscles were stimulated to produce compound action potentials (AP) using a TTL triggered 488nm blue laser (OdicForce Ltd.). Laser light was directed through free space to the muscle and focused onto the muscle using an f=400 mm plano-convex lens, giving a $1/e^2$ laser spot size of $\approx 150\mu$m, measured using a microscope camera mounted above the sample chamber. This beam waist could be further reduced by additional lenses in the beam path as required. Using optomechanical mirror mounts, the laser spot could be moved at sub-millimeter precision to any position on the muscle, with a travel of 2×2 cm^2 across the chamber. This represents an improvement over a confocal/inverted widefield microscopy configuration where stimulation is limited only to the center of the objective field of view[45,46]. We positioned the stimulation laser spot approximately 0.5 mm (Figure 1,b) along the muscle away from the diamond, to ensure we recorded signal propagation in only one direction (towards one end of the muscle). Control measurements were taken of the photovoltaic effect from laser stimulation incident to the probe electrode (see Supplementary Information, SI), and for laser stimulation directly on the diamond. Here, no detectable artifact was observed in the magnetic data, measuring using 5ms pulses at 50mW directly onto the Kapton layer above the diamond for up to 10 hours.

To ensure the stray field from the high current at laser turn-on was not recorded, the blue laser head was placed 3.5m away from the setup and the TTL trigger optically decoupled. Optimal blue laser power was found by initially stimulating the muscle with low input laser power (5 mW), and then slowly increasing the power until a maximal response of the muscle was observed in the electric data. Optical stimulation was performed at a frequency of 0.5 Hz and with a pulse length of 5 ms. For this length, stimulation power was found to be in the range of 20-50 mW, varying between different muscles. Signals were recorded using 60s continuous time traces, giving the high spectral resolution necessary to filter and remove background magnetic noise. Many hours of recording could be acquired, limited by muscle lifespan in the solution bath (up to 20h).

E. Filtering by Spectral Whitening

Without magnetic shielding, it was necessary to remove a substantial amount of magnetic noise from our measurements, including stationary mains noise at harmonics of 50Hz and non-stationary noise from building pumps and compressors. In our previous work, we demonstrated filtering using windowed notch filtering[47]. However this noise removal was suboptimal, due to the use of serially generated fixed frequency windows and a single global threshold value to identify noise peaks, constraints imposed by computational time. Here, we instead implemented a Linear Time-Invariant (LTI) spectral whitening filter. This method has been used for applications including radar and detection of gravitational waves[48–50]. To implement the filter, the power spectral density (PSD) of each 60s time trace was used to estimate the noise spectrum and to derive the transfer function for whitening the signals. The double-sided PSD was calculated with Welch's periodogram method with a segment length of 3.5s and 50% overlap. The input signals were whitened in the range from 20Hz-40kHz; the lower frequency bound was chosen in order to avoid high-pass filter artifacts, the high frequency bound was set by the digitization Nyquist frequency. Following whitening, an additional 3rd order Butterworth 650Hz lowpass filter was applied. Baseline wander was removed from the trials using robust detrending[51]. Further details of the filter method and optimization are supplied in the SI.

F. Simulation and Modelling

In order to verify and analyze the detected signal we performed a numerical simulation of the magnetic field and NV response expected for the muscle biosystem. We use the NEURON package[52] to simulate the signal propagation in a muscle. The ion channel mechanisms were modified in accordance with a previous muscle model on EDL muscles in mice[53] (full details in SI). The optogenetic stimulation current was modeled with the use of a biophysical model developed by Foutz el al.[54] and based on the four-state model described by Nikolic et al.[55].

We modeled the individual muscle fibers in a cylindrical geometry with a cylinder radius of 845 μm and an individual fiber radius given by a uniform distribution of 22.5 ± 3.5 μm[56]. The fibers started at the back end of the laser stimulation spot and extended straight across the laser beam, and over across the NV diamond (Figure 1,b and c). The light distribution inside the muscle was calculated according to the Kubelka-Munk model. The diamond was divided into 20x20 pixels with side-lengths of 100μm, with magnetic field calculated at each pixel, and then averaged across the whole diamond. The local field potential (LFP) was calculated as a monopolar readout approximately at the site of the electrical recording tip (Figure 1,c). The magnetic and electrical field calculation were based on calculations performed in[40], using the LFPy software package[57].

III. RESULTS AND DISCUSSION

We performed *in vitro* studies of EDL muscles dissected from mice, expressing the light sensitive cation channel Channelrhodopsin2 (ChR2) in muscle cells to achieve optogenetic triggering of electrical activity in the muscle using blue light. Muscles were placed in a solution chamber directly above our diamond (Figure 1) and stimulated by a 488nm laser diode in free space, focused using a long working distance lens into the sample chamber. The electrical response (*electric data* in this work) was measured using an AgCl electrode in light surface contact with the muscle (Figure 1) and the induced magnetic field recorded simultaneously by the NV centers in the diamond (*magnetic data* below).

PLEASE CITE THIS ARTICLE AS DOI: 10.1116/5.0106099

A. Movement Inhibition

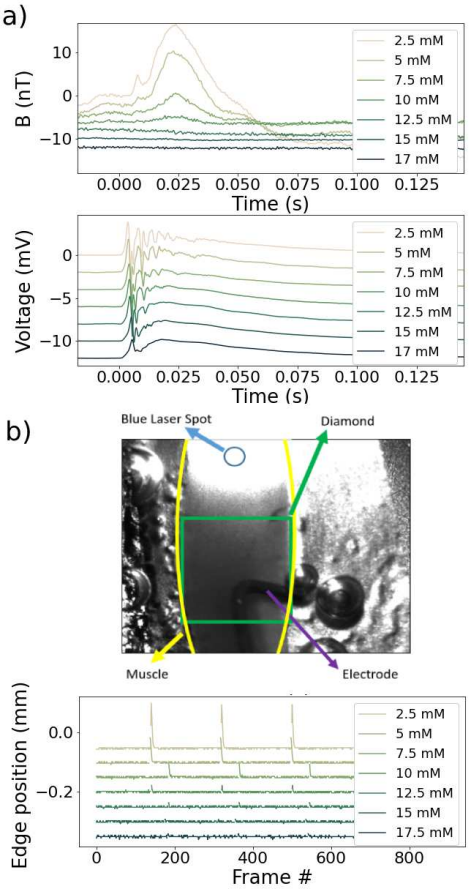

FIG. 2. **Movement artifact elimination by introduction of BDM** a) Magnetic response to stimulation - with low concentrations of BDM a large artifact associated with muscle movement was observed; this was eliminated at concentrations above 15mM. Bottom: Electric data for the same muscle. Here, oscillations arising from movement of the electrode on the moving muscle are reduced in favour of the biosignal of the electrical activity in the muscle. b) To fully confirm the suppression of movement, we used white light microscopy, imaging the muscle edge during stimulation with a camera at 90fps. Above 15mM, spikes associated with muscle movement are completely eliminated.

The strong contraction of the muscle after laser stimulation was found to produce a movement-induced artifact in our magnetic data from the NV centers This artifact arose due to a slight shift in microwave resonance frequency resulting from a motion-induced change in coupling between the nearfield antenna and the diamond and tissue above it. In order to remove this artifact, we pharmacologically suppressed movement using the myosin ATPase inhibitor 2,3-Butanedione monoxime (BDM), without affecting compound action potential propagation. To determine the necessary concentration, we gradually increased the concentration of BDM in the recycled ACSF perfused through the solution bath, starting at 2.5 mM and increasing in steps of 2.5 mM at 10 minute intervals.

Figure 2,a) shows the measured NV sensing response (magnetic data) for a laser stimulated muscle at a range of different concentrations of BDM. With no or low concentration of BDM, we observed a significant movement artifact, equivalent to a 15nT magnetic field signal, followed by a decaying response lasting over 200ms. This artifact completely masked the sought action potential signal from the muscle. The motion artifact was considerably larger for laser stimulation than observed in our previous work using LED stimulation. We attribute this to significantly more effective stimulation of the muscle with the higher intensity laser than the weaker LED light, with the stronger movement clearly visible even by eye.

By increasing the concentration of BDM from 2.5 to 20mM in the ACSF solution, we observed a clear reduction in the movement artifact, with complete elimination above 15mM. This could also be observed in the electric signal from the surface electrode, with oscillations reflecting the movement of the electrode on the muscle eliminated in favor of the electrical response in the muscle (Figure 2, a). In order to confirm the absence of movement, we used a white light microscope and camera mounted above the sample, recording the movement of the muscle edge as a function of time while stimulating with the blue laser. With low concentrations of BDM, clear jumps in position could be observed post-stimulation as the muscle moved (Figure 2,b). Above 15mM of BDM, these were completely suppressed, with no movement detectable anywhere along the muscle.

B. Noise Filtering

In Figure 3,a) and b) we show the unfiltered power spectral density (PSD) from our magnetic data, containing significant noise from background magnetic field sources. We show the effect of our whitening filter algorithm in Figure 3,b), c) and d). As can be observed in the spectrum and the post-filtered timeseries, the filter significantly reduced the noise level. The PSD used to derive the filter was calculated using Welch's method with time intervals of 3.5s, 50% overlap and Hanning window. In Supplementary Information, we outline the process by which we optimise the parameters of the whitening filter to remove noise, while retaining sufficient frequency components of the biosignal. We also directly compare the whitening filter performance against that derived using notch filtering and clarify how real absolute magnetic field units (Tesla) can be recovered from the relative PSD of the whitened data. Overall, we found the performance of the whitening filter in terms of noise removal was not significantly better than by using the notch filter method. However, it was significantly

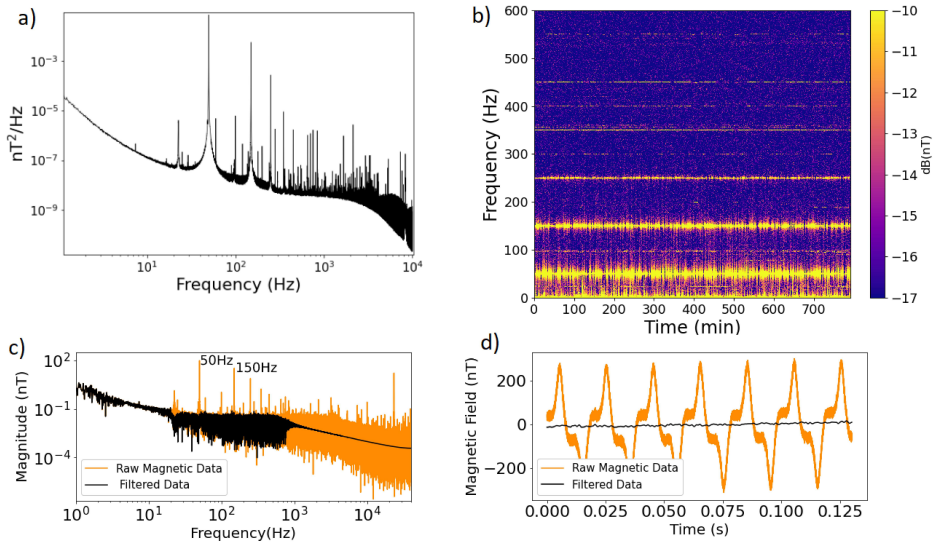

FIG. 3. **Reduction of magnetic noise through post-processing filtering** a) Averaged spectrum of the background magnetic data noise as seen by NV centers and b) spectrogram of the same noise taken over 13 hours (normalized to 1nT). We observe significant noise arising from sources such as mains electricity in the <1kHz region that contains the majority of the components of the ms-scale biological signal. c) Comparison of the amplitude spectrum before and after the application of the whitening filter, with a significant amount of noise identified and removed. This is reflected in the example timeseries shown in d), showing a 0.5sec trace before and after the filter is implemented. Filtering reduces the noise from peak-to-peak of 400nT to less than 1nT on a single 60sec trace.

PLEASE CITE THIS ARTICLE AS DOI: 10.1116/5.0106099

faster ($\times$2.5 speedup) and easier to implement, requiring only the calculation of the PSD for each 60s time trace compared to a serial algorithm needed to sweep through and build the notch filter mask. We found this could also be sped up by performing an initial time domain filter step via principle component analysis of the raw signal[58](see SI). For the majority of biological applications, the signal shape and relative amplitude is of main concern, making the whitening method a fast and effective option.

C. Biosignal Readout

In Figure 4 we show examples of the biological signal measured using NV sensing (*magnetic data*) and simultaneously recorded electrically using the AgCl contact electrode (*electric data*) for 3 different muscles (M1-3), each recorded in a separate experimental run. For each muscle, we observed both a fast response peak (AP) at $\sim$5ms and a slower response (CH) at $\sim$10ms after the stimulation trigger. Based on our modelling (see below) and earlier results in the literature, we interpret the first peak (AP) to the compound action potential response and the second slower peak (CH) to the response from channelrhodopsin activity[59,60]. Both signals decayed in amplitude over many stimulations while retaining a similar shape, with the AP signal decaying more rapidly and begin subsumed into the CH signal after 4-6 hours of measurement (Figure 5). A slight delay in time was observed between the electric and magnetic data, arising from the positioning of the probe electrode away from the stimulation site, but still within 0.2-0.5 mm of the 2 $\times$2 mm^2 diamond. We use a compromise upper cutoff frequency of 650Hz, minimizing distortion to both AP and CH signals (see SI), but acting to smooth the AP signal in the magnetic data.

We note that the biological signal we observe using laser stimulation is significantly different from that previously observed for LED stimulation[42]. The AP peak amplitude was weaker by a factor of 2 and in both the electric and magnetic data and recording shown in Figure 2, a), we observed a non-negative refractory period followed by a slowly (tens of milliseconds) decaying response (CH). Furthermore, we observe a difference in the relative height of the AP and CH peaks between the magnetic and electrical readouts. We attribute this to the channelrhodopsin channels opening faster and remaining open for longer under higher intensity laser light, allowing ionic current to flow for longer and generating the strong CH signal.

The peak magnetic field observed for muscle M2 was a factor of 5 stronger than for M1 and M3. We consider this likely to arise due to unexpected variability in NV response across the 2 $\times$2 mm^2 diamond area. Due to the high level of internal reflection in high refractive index diamond, that we col-

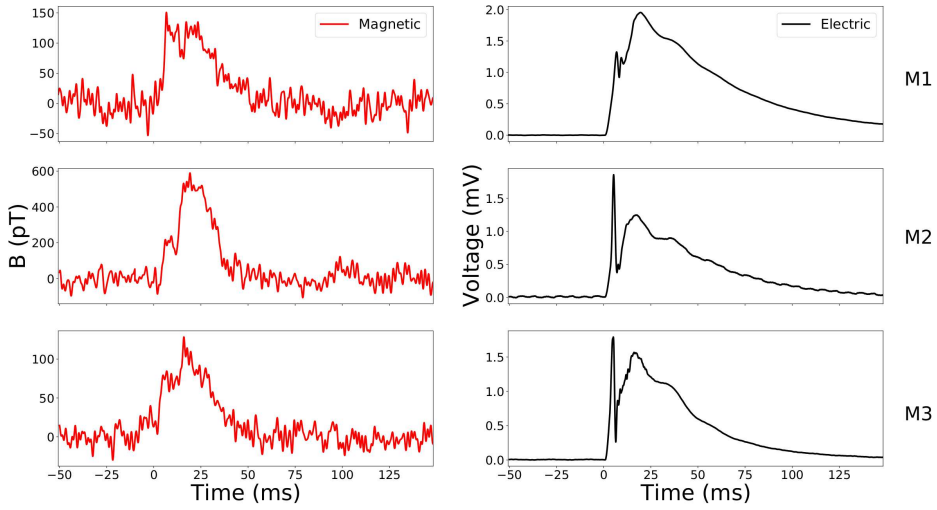

FIG. 4. **Measuring the muscle biological response electrically and magnetically**. Magnetic and electric data recorded for 3 different muscles (M1-M3). The data shown is the average response over 15000, 13500 and 540 stimulations (8h, 7.5h and 18 min of 60s acquisitions, with a 0.5Hz stimulation rate) for M1-3 respectively. The action potential (AP) peak and the channelrhodopsin (CH) are clearly distinguishable on all three muscles. On all subfigures, time t=0 corresponds to the instant laser stimulation is triggered.

PLEASE CITE THIS ARTICLE AS DOI: 10.1116/5.0106099

lect light from the full diamond volume and that the diamond had a relatively uniform density of NV centers, we expected NV sensitivity to magnetic field to not vary significantly depending on muscle position, so long as the muscle was positioned approximately above the diamond. However, we found this not to be the case. Later investigations using a scanned electrified probe tip across the diamond surface, recording the magnetic field it induced, determined an area approximately 0.5×0.5 mm to be a factor 16 better sensitivity than the lowest response elsewhere on the diamond (see SI). This region corresponded approximately to where the pump laser beam struck the diamond, receiving the maximum laser intensity.

Although we cannot directly confirm the precise positioning, in the case of M2 it is likely the muscle was located optimally at the most sensitive region. For M1 and M2, the location was suboptimal but enough to yield a signal. We consider the positional response a particularly important result for NV sensing, highlighting the need to correctly position the biosamples and spatially map response across the diamond. We also highlight that this potentially offers a novel route to spatially resolve and image signals well below the physical dimensions of the diamond. Using a scanned, highly focused pump laser beam, the point of maximum field sensitivity could be moved across the diamond, allowing recording from different areas of the sample above. Although implementation is beyond the scope of this work, such a scheme could be realised using galvanic mirrors or electro/acousto-optic beam scanning for higher speeds.

D. Simulation and Modeling

In order to explore the origin of the observed signal features, we modeled the muscle system to calculate the response under laser stimulation[52–54,57]. Full model details are given in the SI. In both electric and magnetic data, we observed a signal (CH) with a slow decay (Figure 4). We attribute this signal to the activation of channelrhodopsin, with such a signal previously observed for optogenetically stimulated muscle signals[59,61]. When trying to model this response, we found that the original biophysical models of ChR2, developed for stimulation of neurons rather than muscle, could not describe the length of the CH signal we observe. Modeling the dynamics of ChR2 in neurons for a large span of different scenarios, including covering the range of current and intensity in this work, predict that any signal should decay within 15 ms of the stimulation[55].

The four-state ChR2 model[62] for this process is shown in Figure 6,a). The ChR2-proteins are mainly populated at rest in the closed fast state (C1), which, when illuminated, transitions to the open fast state (O1) with transition rate K_{a1} (stimulation laser intensity dependent) thus allowing influx of ions to the fiber. The O1 is unstable and decays mainly to C1 (with transition rate K_{d1}) as long as short excitation pulses ($\approx$5 ms) are used. This typically results in a single action potential without any pronounced secondary prolonged current.

With longer pulse duration, C1 can also transition to the slow opened state (O2). This transition is characterized with the irradiance dependent transition rates e_{12} and e_{21}. The O2

PLEASE CITE THIS ARTICLE AS DOI: 10.1116/5.0106099

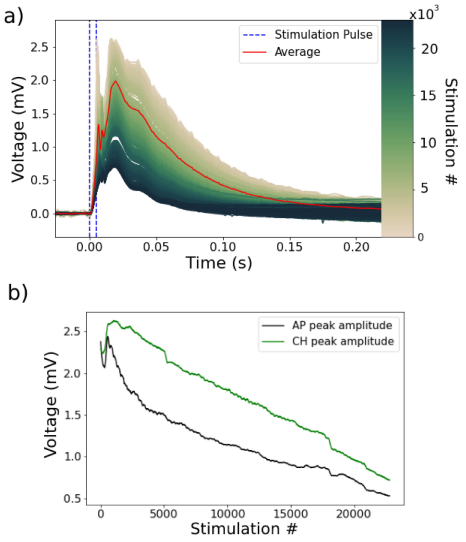

FIG. 5. **Stability of the measured biological response over time**. a) Variations in electric data recording versus number of stimulations for muscle M1. The amplitude of the signal gradually decreased over time as the muscle fatigued. We observed both a fast response peak from the action potential at ∼5ms and a second slower peak from channelrhodopsin at ∼20ms. b) Scaling of the standard deviation of the 60s timeseries (measuring noise) as a function of number of stimulations for both notch and whitening filtering, showing the decay of the AP and CH peaks.

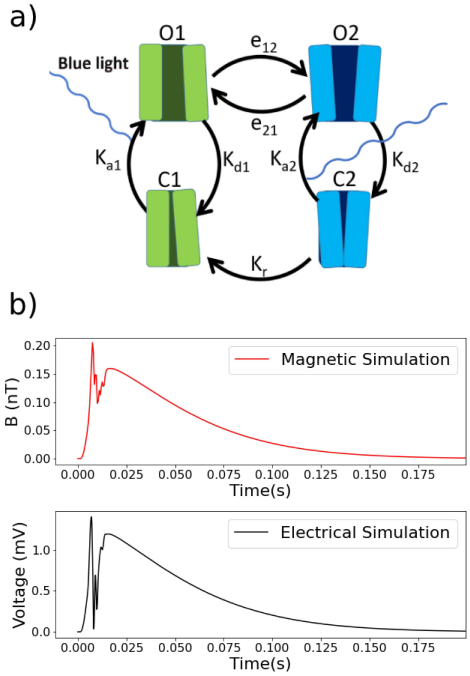

FIG. 6. **Simulations of channelrhodopsin behaviour**. a) Depiction of the different stages of the four-state model of a ChR2 molecule. Blue light can transition the ChR2 from closed (C1 and C2) to open (O1 and O2). b) Upper figure show simulated magnetic signal as detected by averaging over the whole diamond. Lower figure show simulated LFP as detected by an electrode positioned as in Figure 1,c. Stimulation is modeled to occur at t=0.

state relaxes relatively slow to the closed slow state (C2) with a transition rate of K_{d2}, which in turn can either transition back to O2 given an excitation, with transition rate K_{a2}, or return to C1 with transition rate K_r. As the O2 state stays open for a longer time period after the stimulation pulse, it also creates a longer decay of the signal. This was experimentally observed for neuron stimulation for excitation pulses exceeding 50ms[55].

However, we observe our slowly decaying CH signal at a shorter stimulation period of 5 ms. This suggests that the ChR2 in the studied muscle transitioned into the O2 state with larger proportion than in neurons. We therefore modified the four-state model to account for this behavior (see SI for full details). Briefly, we modeled the induction of a secondary long-lasting current at a stimulation period of 5 ms by allowing for a stronger transition to the O2 configuration in ChR2, decaying more slowly to the closed state. This was done by setting the e_{12} and e_{21} parameters higher during illumination, and then letting e_{12} remain high after illumination, whereas e_{21} returned to a low value (Table SI2). Furthermore, the conductivity of the O2 state was also set higher than in previous models (from about 2-5fS to 25fS). These alternative values for the ChR2 model are justified by considering that the original ChR2 model was developed and tested for systems with lower stimulation intensities and for neuronal structures instead of muscle. Modification of these few parameters gives a modeled signal (Figure 6, b) highly representative of the magnetic and electric data recorded experimentally (Figure 4).

IV. CONCLUSIONS

We seek in this experiment to demonstrate the viability of using high intensity, focused laser stimulation of dissected living tissue *in vitro* while recovering biosignals at the microscopic level using a quantum sensor. Although we use simple muscle tissue as proof of principle, which could be easily probed electrically, our results show that highly localized, high intensity, selective excitation of specific biological processes in more complex systems can be done while passively sensing in the same localized region. This is a step towards realizing proposals such as mapping neural activity

PLEASE CITE THIS ARTICLE AS DOI: 10.1116/5.0106099

in networks in the brain[63] and experiments using intracellular nanodiamonds[64], where highly focused stimulation will be necessary. We note our method is at the early stages of development and does not seek to compete with well-developed alternatives (e.g. multiprobe arrays, Ca^{2+} imaging), with future improvement in sensitivity required to realize these goals. We highlight that our sensing is entirely passive, requiring no direct mechanical contact or laser light into the tissue, and thus avoids issues with variability of electrical conductivity and optical transparency that are detrimental to established techniques. NV sensing relies on fundamental physical principles and is not limited to optogenetic stimulation in genetically modified organisms.

Our results show that laser optogenetic stimulation of muscle tissue evokes a strong physical response, producing a significant movement artifact in the magnetic data readout from the NV centers. We were able to fully suppress this artifact using a pharmacological muscle movement inhibitor, although suppression was challenging with higher intensity laser illumination. This aspect should be considered closely for any future experiments with high intensity laser stimulation, which may produce unwanted artifacts. Although in this work the motion artifact represented a disadvantage, it could be exploited for force/motion detection using color centers, such as vector sensing of force/movement in a biological sample[65].

In both the electric and the magnetic data we record, we observe both short period (AP) and long period (CH) signals. Through modeling, we interpret these signals to muscle action potential (AP) and to current flow through channelrhodopsin (CH), with more muscle fibers addressed by the deeply penetrating laser beam and the channel opened for longer by the higher laser intensity. In order to further test the origins of the respective signals, it would be necessary to inhibit the action potential using pharmacology. Unfortunately, we were unable to perform such experiments in this work. Although not ideal, with the channelrodopsin activation obscuring the action potential signal, the result exemplifies the usefulness of NV sensing in gaining new insight into a biological system close to the optical stimulation site. Using alternative techniques, artifacts arising from photovoltaic effects (for electrical probes) or optical bleaching (for fluorescent biomarkers) would entirely mask the biosignal. The muscle position variability of the strength of our magnetic response highlights the need to properly characterize the response and sensitivity across the diamond, and the potential to record strong signals if this process is well optimized. These results also potentially point to a way to achieve spatial resolution below the physical dimensions of the diamond, while still maintaining the same optical collection and excitation scheme. Such spatial resolution is key to fully, microscopically resolve and identify the origin of activity in living biological samples.

Through spectral whitening filtering we achieve a high degree of rejection of background magnetic noise, comparable in noise reduction performance as for using a notch bandstop filters[42,47], but with significant improvement in terms of post-processing filter time ($\approx$2.5 times faster), especially where recovery of precise field units are not required. Processing speed could be further enhanced by an initial time domain filter step using principle component analysis to remove the main noise components (e.g. 50/150Hz inductive mains). Further advances in filtering may be obtained by implementing artificial intelligence techniques in filter design, in particular by supplying synthetic known biosignals and optimizing the response of the NV ensemble to these signals. These capabilities represent a step forward in terms of realizing real-time biological signal recovery in an ordinary, unshielded lab or clinical environment, key to the study of living biological systems.

V. COMPETING INTERESTS

Hartwig R. Siebner has received honoraria as speaker from Sanofi Genzyme, Denmark and Novartis, Denmark, as consultant from Sanofi Genzyme, Denmark, Lophora, Denmark, and Lundbeck AS, Denmark, and as editor-in-chief (Neuroimage Clinical) and senior editor (NeuroImage) from Elsevier Publishers, Amsterdam, The Netherlands and royalties as book editor from Springer Publishers, Stuttgart, Germany and from Gyldendal Publishers, Copenhagen, Denmark.

VI. ETHICAL STATEMENT

The work described in this article has been carried out in accordance with Directive 86/609/EEC for animal experiments and all relevant national legislation in Denmark.

VII. SUPPLEMENTARY MATERIAL

See supplementary material at [URL will be inserted by AIP Publishing] for supplementary data and figures in support of the main text.

ACKNOWLEDGMENTS

This work was funded by the Novo Nordisk foundation through the synergy grant bioQ (Grant Number: NNF17OC0028086), BIO-MAG (NNF21OC0066526) and the Center for Macroscale Quantum States (bigQ) funded by the Danish National Research Foundation (Grant number:DNRF142). Hartwig R. Siebner holds a 5-year professorship in precision medicine at the Faculty of Health Sciences and Medicine, University of Copenhagen funded by the Lundbeck Foundation (Grant Nr. R186).

DATA AVAILABILITY STATEMENT

The data that support the findings of this study are available from the corresponding author upon reasonable request.

PLEASE CITE THIS ARTICLE AS DOI: 10.1116/5.0106099

[1] C. M. McDonald, "Clinical approach to the diagnostic evaluation of hereditary and acquired neuromuscular diseases," Physical Medicine and Rehabilitation Clinics of North America **23**, 495–563 (2012), neuromuscular Disease Management and Rehabilitation, Part I: Diagnostic and Therapy Issues.

[2] M. Scanziani and M. HÃusser, "Electrophysiology in the age of light," Nature **461**, 930–939 (2009).

[3] C. Grienberger and A. Konnerth, "Imaging calcium in neurons," Neuron **73**, 862–885 (2012).

[4] M. Z. Lin and M. J. Schnitzer, "Genetically encoded indicators of neuronal activity," Nat. Neurosci. **19**, 1142–1153 (2016).

[5] A. Gechev, N. Kane, M. Koltzenburg, D. Rao, and R. van der Star, "Potential risks of iatrogenic complications of nerve conduction studies (ncs) and electromyography (emg)," Clinical Neurophysiology Practice **1**, 62–66 (2016).

[6] S. Mahajan, J. K. Hermann, H. W. Bedell, J. A. Sharkins, L. Chen, K. Chen, S. M. Meade, C. S. Smith, J. Rayyan, H. Feng, Y. Kim, M. A. Schiefer, D. M. Taylor, J. R. Capadona, and E. S. Ereifej, "Toward standardization of electrophysiology and computational tissue strain in rodent intracortical microelectrode models," Frontiers in Bioengineering and Biotechnology **8**, 416 (2020).

[7] J. Clarke, Y.-H. Lee, and J. Schneiderman, "Focus on SQUIDs in biomagnetism," Superconductor Science and Technology **31**, 080201 (2018).

[8] M. Hämäläinen, R. Hari, R. J. Ilmoniemi, J. Knuutila, and O. V. Lounasmaa, "Magnetoencephalography—theory, instrumentation, and applications to noninvasive studies of the working human brain," Reviews of Modern Physics **65**, 413–497 (1993).

[9] J. Arlett, E. Myers, and M. Roukes, "Comparative advantages of mechanical biosensors," Nature nanotechnology **6**, 203–215 (2011).

[10] D. R. Baselt, G. U. Lee, M. Natesan, S. W. Metzger, P. E. Sheehan, and R. J. Colton, "A biosensor based on magnetoresistance technology," Biosensors and Bioelectronics **13**, 731–739 (1998).

[11] E. Boto, N. Holmes, J. Leggett, G. Roberts, V. Shah, S. S. Meyer, L. D. Muñoz, K. J. Mullinger, T. M. Tierney, S. Bestmann, G. R. Barnes, R. Bowtell, and M. J. Brookes, "Moving magnetoencephalography towards real-world applications with a wearable system," Nature **555**, 657–661 (2018).

[12] W. Liu, M. N. A. Alam, Y. Liu, V. N. Agafonov, H. Qi, K. Koynov, V. A. Davydov, R. Uzbekov, U. Kaiser, T. Lasser, F. Jelezko, A. Ermakova, and T. Weil, "Silicon-vacancy nanodiamonds as high performance near-infrared emitters for live-cell dual-color imaging and thermometry," Nano Letters **22**, 2881–2888 (2022).

[13] J. M. Taylor, P. Cappellaro, L. Childress, L. Jiang, D. Budker, P. R. Hemmer, A. Yacoby, R. Walsworth, and M. D. Lukin, "High-sensitivity diamond magnetometer with nanoscale resolution," Nature Physics **4**, 810–816 (2008).

[14] F. Dolde, H. Fedder, M. W. Doherty, T. Nöbauer, F. Rempp, G. Balasubramanian, T. Wolf, F. Reinhard, L. C. L. Hollenberg, F. Jelezko, and J. Wrachtrup, "Electric-field sensing using single diamond spins," Nature Physics **7**, 459–463 (2011).

[15] P. Neumann, I. Jakobi, F. Dolde, C. Burk, R. Reuter, G. Waldherr, J. Honert, T. Wolf, A. Brunner, J. H. Shim, D. Suter, H. Sumiya, J. Isoya, and J. Wrachtrup, "High-precision nanoscale temperature sensing using single defects in diamond," Nano Letters **13**, 2738–2742 (2013).

[16] P. Kehayias, M. J. Turner, R. Trubko, J. M. Schloss, C. A. Hart, M. Wesson, D. R. Glenn, and R. L. Walsworth, "Imaging crystal stress in diamond using ensembles of nitrogen-vacancy centers," Physical Review B **100** (2019).

[17] P. Neumann, R. Kolesov, V. Jacques, J. Beck, J. Tisler, A. Batalov, L. Rogers, N. B. Manson, G. Balasubramanian, F. Jelezko, and J. Wrachtrup, "Excited-state spectroscopy of single NV defects in diamond using optically detected magnetic resonance," New Journal of Physics **11**, 013017 (2009).

[18] S. Steinert, F. Dolde, P. Neumann, A. Aird, B. Naydenov, G. Balasubramanian, F. Jelezko, and J. Wrachtrup, "High sensitivity magnetic imaging using an array of spins in diamond," Review of Scientific Instruments **81**, 043705 (2010).

[19] I. Fescenko, A. Jarmola, I. Savukov, P. Kehayias, J. Smits, J. Damron, N. Ristoff, N. Mosavian, and V. M. Acosta, "Diamond magnetometer enhanced by ferrite flux concentrators," Physical Review Research **2** (2020).

[20] T. Wolf, P. Neumann, K. Nakamura, H. Sumiya, T. Ohshima, J. Isoya, and J. Wrachtrup, "Subpicotesla diamond magnetometry," Physical Review X **5** (2015).

[21] Y. Wu and T. Weil, "Recent developments of nanodiamond quantum sensors for biological applications," Advanced Science **9**, 2200059 (2022).

[22] K. Mizuno, H. Ishiwata, Y. Masuyama, T. Iwasaki, and M. Hatano, "Simultaneous wide-field imaging of phase and magnitude of AC magnetic signal using diamond quantum magnetometry," Scientific Reports **10** (2020).

[23] D. L. Sage, K. Arai, D. R. Glenn, S. J. DeVience, L. M. Pham, L. Rahn-Lee, M. D. Lukin, A. Yacoby, A. Komeili, and R. L. Walsworth, "Optical magnetic imaging of living cells," Nature **496**, 486–489 (2013).

[24] J. F. Barry, J. M. Schloss, E. Bauch, M. J. Turner, C. A. Hart, L. M. Pham, and R. L. Walsworth, "Sensitivity optimization for NV-diamond magnetometry," Reviews of Modern Physics **92** (2020).

[25] D. Toyli, D. Christle, A. Alkauskas, B. Buckley, C. Van de Walle, and D. Awschalom, "Measurement and control of single nitrogen-vacancy center spins above 600 k," Physical Review X **2**, 031001 (2012).

[26] G. Petrini, G. Tomagra, E. Bernardi, E. Moreva, P. Traina, A. Marcantoni, F. Picollo, K. Kvaková, P. Cígler, I. P. Degiovanni, V. Carabelli, and M. Genovese, "Nanodiamond–quantum sensors reveal temperature variation associated to hippocampal neurons firing," Advanced Science , 2202014 (2022).

[27] J. F. Barry, M. J. Turner, J. M. Schloss, D. R. Glenn, Y. Song, M. D. Lukin, H. Park, and R. L. Walsworth, "Optical magnetic detection of single-neuron action potentials using quantum defects in diamond," Proceedings of the National Academy of Sciences **113**, 14133–14138 (2016).

[28] Y. Wu, M. N. A. Alam, P. Balasubramanian, A. Ermakova, S. Fischer, H. Barth, M. Wagner, M. Raabe, F. Jelezko, and T. Weil, "Nanodiamond theranostic for light-controlled intracellular heating and nanoscale temperature sensing," Nano Lett. **21**, 3780–3788 (2021).

[29] A. Horsley, P. Appel, J. Wolters, J. Achard, A. Tallaire, P. Maletinsky, and P. Treutlein, "Microwave device characterization using a widefield diamond microscope," Phys. Rev. Applied **10**, 044039 (2018).

[30] A. Gruber, A. DrÃbenstedt, C. Tietz, L. Fleury, J. Wrachtrup, and C. von Borczyskowski, "Scanning confocal optical microscopy and magnetic resonance on single defect centers," Science **276**, 2012–2014 (1997).

[31] T. D. Y. Kozai and A. L. Vazquez, "Photoelectric artefact from optogenetics and imaging on microelectrodes and bioelectronics: new challenges and opportunities," J. Mater. Chem. B Mater. Biol. Med. **3**, 4965–4978 (2015).

[32] J. A. Cardin, M. Carlén, K. Meletis, U. Knoblich, F. Zhang, K. Deisseroth, L.-H. Tsai, and C. I. Moore, "Targeted optogenetic stimulation and recording of neurons in vivo using cell-type-specific expression of channelrhodopsin-2," Nat. Protoc. **5**, 247–254 (2010).

[33] A. M. Packer, B. Roska, and M. Hausser, "Targeting neurons and photons for optogenetics," Nat. Neurosci. **16**, 805–815 (2013).

[34] T. Staudacher, F. Shi, S. Pezzagna, J. Meijer, J. Du, C. A. Meriles, F. Reinhard, and J. Wrachtrup, "Nuclear magnetic resonance spectroscopy on a (5-nanometer)3 sample volume," Science **339**, 561–563 (2013).

[35] J. Xu, L. E. Jarocha, T. Zollitsch, M. Konowalczyk, K. B. Henbest, S. Richert, M. J. Golesworthy, J. Schmidt, V. Déjean, D. J. C. Sowood, M. Bassetto, J. Luo, J. R. Walton, J. Fleming, Y. Wei, T. L. Pitcher, G. Moise, M. Herrmann, H. Yin, H. Wu, R. Bartölke, S. J. Käsehagen, S. Horst, G. Dautaj, P. D. F. Murton, A. S. Gehrckens, Y. Chelliah, J. S. Takahashi, K.-W. Koch, S. Weber, I. A. Solov'yov, C. Xie, S. R. Mackenzie, C. R. Timmel, H. Mouritsen, and P. J. Hore, "Magnetic sensitivity of cryptochrome 4 from a migratory songbird," Nature **594**, 535–540 (2021).

[36] G. Kucsko, P. C. Maurer, N. Y. Yao, M. Kubo, H. J. Noh, P. K. Lo, H. Park, and M. D. Lukin, "Nanometre-scale thermometry in a living cell," Nature **500**, 54–58 (2013).

[37] M. Fujiwara, S. Sun, A. Dohms, Y. Nishimura, K. Suto, Y. Takezawa, K. Oshimi, L. Zhao, N. Sadzak, Y. Umehara, Y. Teki, N. Komatsu, O. Benson, Y. Shikano, and E. Kage-Nakadai, "Real-time nanodiamond thermometry probing in vivo thermogenic responses," Science Advances **6**, eaba9636 (2020).

[38] L. P. McGuinness, Y. Yan, A. Stacey, D. A. Simpson, L. T. Hall, D. Maclaurin, S. Prawer, P. Mulvaney, J. Wrachtrup, F. Caruso, R. E. Scholten, and L. C. L. Hollenberg, "Quantum measurement and orientation tracking of fluorescent nanodiamonds inside living cells," Nature Nanotechnology **6**, 358–363 (2011).

[39]L. T. Hall, G. C. G. Beart, E. A. Thomas, D. A. Simpson, L. P. McGuinness, J. H. Cole, J. H. Manton, R. E. Scholten, F. Jelezko, J. Wrachtrup, S. Petrou, and L. C. L. Hollenberg, "High spatial and temporal resolution wide-field imaging of neuron activity using quantum NV-diamond," Scientific Reports **2** (2012).

[40]M. Karadas, A. M. Wojciechowski, A. Huck, N. O. Dalby, U. L. Andersen, and A. Thielscher, "Feasibility and resolution limits of opto-magnetic imaging of neural network activity in brain slices using color centers in diamond," Scientific Reports **8** (2018).

[41]J. C. Price, R. Mesquita-Ribeiro, F. Dajas-Bailador, and M. L. Mather, "Widefield, spatiotemporal mapping of spontaneous activity of mouse cultured neuronal networks using quantum diamond sensors," Frontiers in Physics **8** (2020).

[42]J. L. Webb, L. Troise, N. W. Hansen, C. Olsson, A. M. Wojciechowski, J. Achard, O. Brinza, R. Staacke, M. Kieschnick, J. Meijer, A. Thielscher, J.-F. Perrier, K. Berg-Sørensen, A. Huck, and U. L. Andersen, "Detection of biological signals from a live mammalian muscle using an early stage diamond quantum sensor," Scientific Reports **11** (2021).

[43]H. A. R. El-Ella, S. Ahmadi, A. M. Wojciechowski, A. Huck, and U. L. Andersen, "Optimised frequency modulation for continuous-wave optical magnetic resonance sensing using nitrogen-vacancy ensembles," Optics Express **25**, 14809 (2017).

[44]K. Sasaki, Y. Monnai, S. Saijo, R. Fujita, H. Watanabe, J. Ishi-Hayase, K. M. Itoh, and E. Abe, "Broadband, large-area microwave antenna for optically detected magnetic resonance of nitrogen-vacancy centers in diamond," Review of Scientific Instruments **87**, 053904 (2016).

[45]M. Mrózek, D. Rudnicki, P. Kehayias, A. Jarmola, D. Budker, and W. Gawlik, "Longitudinal spin relaxation in nitrogen-vacancy ensembles in diamond," EPJ Quantum Technology **2** (2015).

[46]E. Bernardi, E. Moreva, P. Traina, G. Petrini, S. D. Tchernij, J. Forneris, Ž. Pastuović, I. P. Degiovanni, P. Olivero, and M. Genovese, "A biocompatible technique for magnetic field sensing at (sub)cellular scale using nitrogen-vacancy centers," EPJ Quantum Technology **7** (2020).

[47]J. L. Webb, L. Troise, N. W. Hansen, J. Achard, O. Brinza, R. Staacke, M. Kieschnick, J. Meijer, J.-F. Perrier, K. Berg-Sørensen, A. Huck, and U. L. Andersen, "Optimization of a diamond nitrogen vacancy centre magnetometer for sensing of biological signals," Frontiers in Physics **8** (2020).

[48]H. Gabbard, M. Williams, F. Hayes, and C. Messenger, "Matching matched filtering with deep networks for gravitational-wave astronomy," Physical Review Letters **120** (2018).

[49]K. Chatziioannou, C.-J. Haster, T. B. Littenberg, W. M. Farr, S. Ghonge, M. Millhouse, J. A. Clark, and N. Cornish, "Noise spectral estimation methods and their impact on gravitational wave measurement of compact binary mergers," Physical Review D **100** (2019).

[50]J. Roman, M. Rangaswamy, D. Davis, Q. Zhang, B. Himed, and J. Michels, "Parametric adaptive matched filter for airborne radar applications," IEEE Transactions on Aerospace and Electronic Systems **36**, 677–692 (2000).

[51]A. de Cheveigné and D. Arzounian, "Robust detrending, rereferencing, outlier detection, and inpainting for multichannel data," NeuroImage **172**, 903–912 (2018).

[52]M. L. Hines and N. T. Carnevale, "Neuron: A tool for neuroscientists," The Neuroscientist **7**, 123–135 (2001).

[53]S. Cannon, R. Brown, and D. Corey, "Theoretical reconstruction of myotonia and paralysis caused by incomplete inactivation of sodium channels," Biophysical Journal **65**, 270–288 (1993).

[54]T. J. Foutz, R. L. Arlow, and C. C. McIntyre, "Theoretical principles underlying optical stimulation of a channelrhodopsin-2 positive pyramidal neuron," Journal of Neurophysiology **107**, 3235–3245 (2012).

[55]K. Nikolic, N. Grossman, M. S. Grubb, J. Burrone, C. Toumazou, and P. Degenaar, "Photocycles of channelrhodopsin-2," Photochemistry and Photobiology **85**, 400–411 (2009).

[56]V. Augusto, C. R. Padovani, and G. E. R. Campos, "Skeletal muscle fiber types in C57BL6J mice," Journal of Morphological Sciences **21**, 0 (2017).

[57]H. Lindén, E. Hagen, S. Leski, E. S. Norheim, K. H. Pettersen, and G. T. Einevoll, "LFPy: a tool for biophysical simulation of extracellular potentials generated by detailed model neurons," Frontiers in neuroinformatics **7**, 41 (2014).

[58]M. Negishi, M. Abildgaard, T. Nixon, and R. T. Constable, "Removal of time-varying gradient artifacts from EEG data acquired during continuous fMRI," Clinical Neurophysiology **115**, 2181–2192 (2004).

[59]T. Bruegmann, T. van Bremen, C. C. Vogt, T. Send, B. K. Fleischmann, and P. Sasse, "Optogenetic control of contractile function in skeletal muscle," Nature Communications **6** (2015).

[60]G. Nagel, M. Brauner, J. F. Liewald, N. Adeishvili, E. Bamberg, and A. Gottschalk, "Light activation of channelrhodopsin-2 in excitable cells of caenorhabditis elegans triggers rapid behavioral responses," Current Biology **15**, 2279–2284 (2005).

[61]P. Magown, B. Shettar, Y. Zhang, and V. F. Rafuse, "Direct optical activation of skeletal muscle fibres efficiently controls muscle contraction and attenuates denervation atrophy," Nature Communications **6** (2015).

[62]N. Grossman, K. Nikolic, C. Toumazou, and P. Degenaar, "Modeling study of the light stimulation of a neuron cell with channelrhodopsin-2 mutants," IEEE Transactions on Biomedical Engineering **58**, 1742–1751 (2011).

[63]A. P. Alivisatos, M. Chun, G. M. Church, R. J. Greenspan, M. L. Roukes, and R. Yuste, "The brain activity map project and the challenge of functional connectomics," Neuron **74**, 970–974 (2012).

[64]R. Schirhagl, K. Chang, M. Loretz, and C. L. Degen, "Nitrogen-vacancy centers in diamond: nanoscale sensors for physics and biology," Annual review of physical chemistry **65**, 83–105 (2014).

[65]D. Cohen, R. Nigmatullin, O. Kenneth, F. Jelezko, M. Khodas, and A. Retzker, "Utilising NV based quantum sensing for velocimetry at the nanoscale," Scientific Reports **10** (2020).

PLEASE CITE THIS ARTICLE AS DOI: 10.1116/5.0106099

PLEASE CITE THIS ARTICLE AS DOI: 10.1116/5.0106099

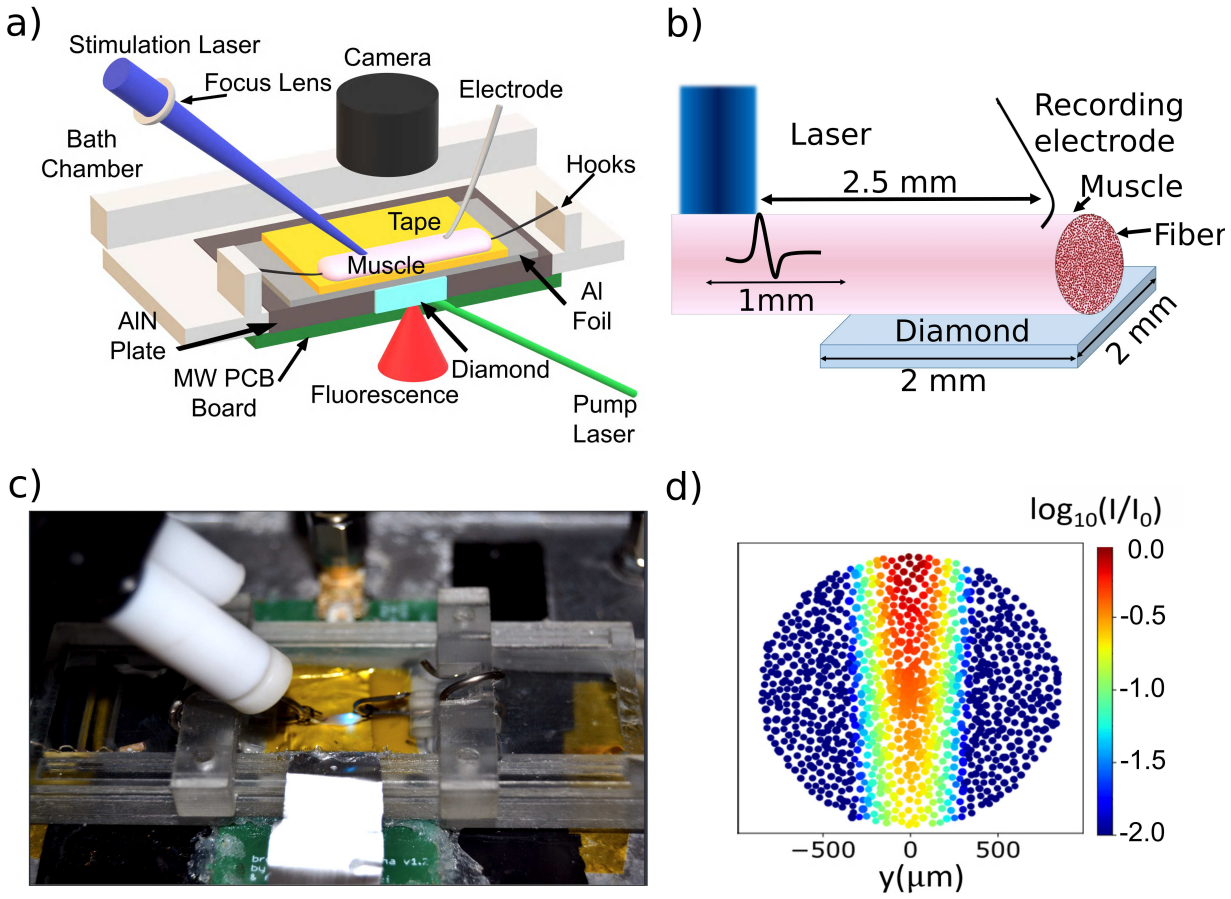

PLEASE CITE THIS ARTICLE AS DOI: 10.1116/5.0106099

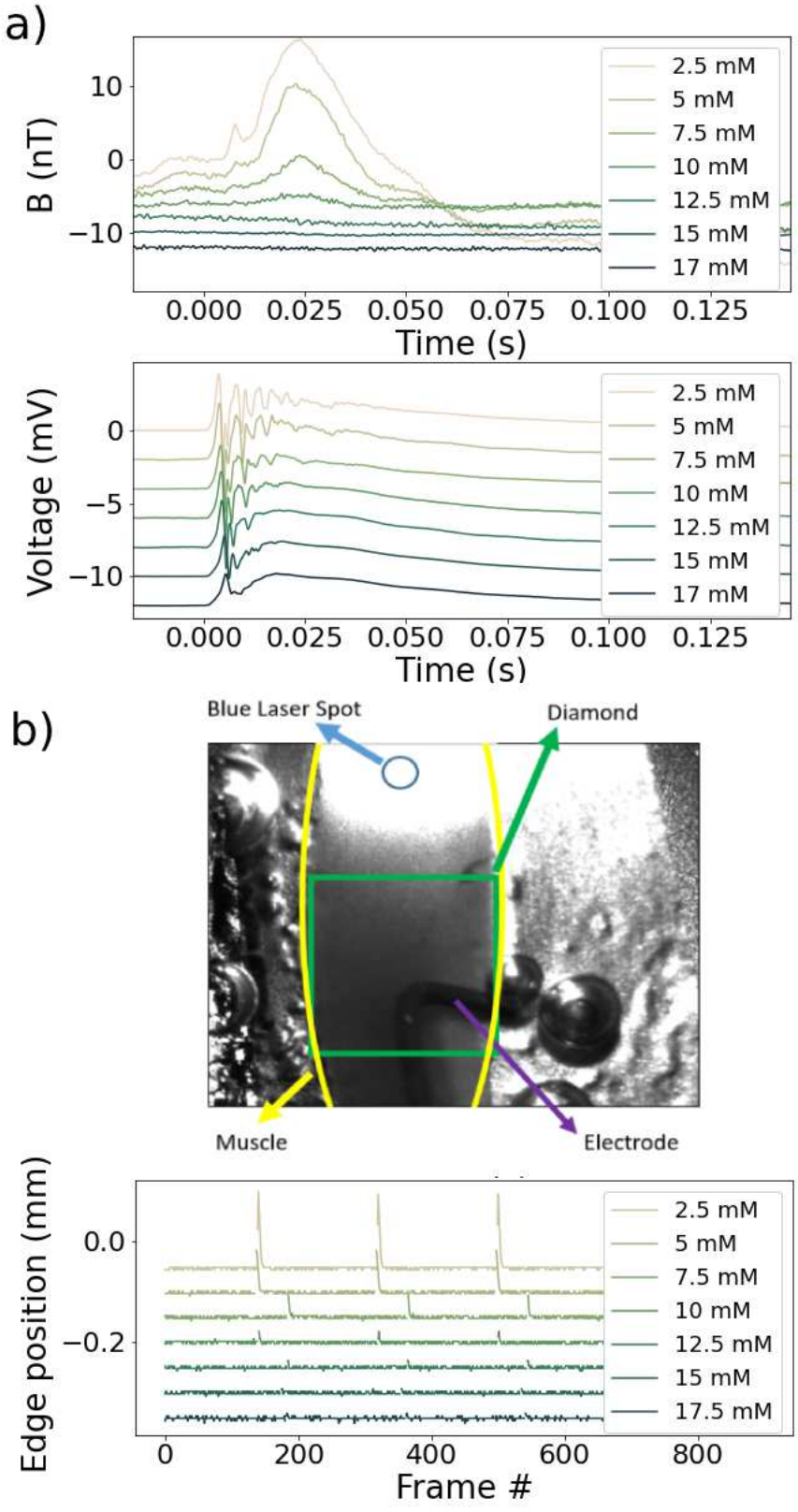

PLEASE CITE THIS ARTICLE AS DOI: 10.1116/5.0106099

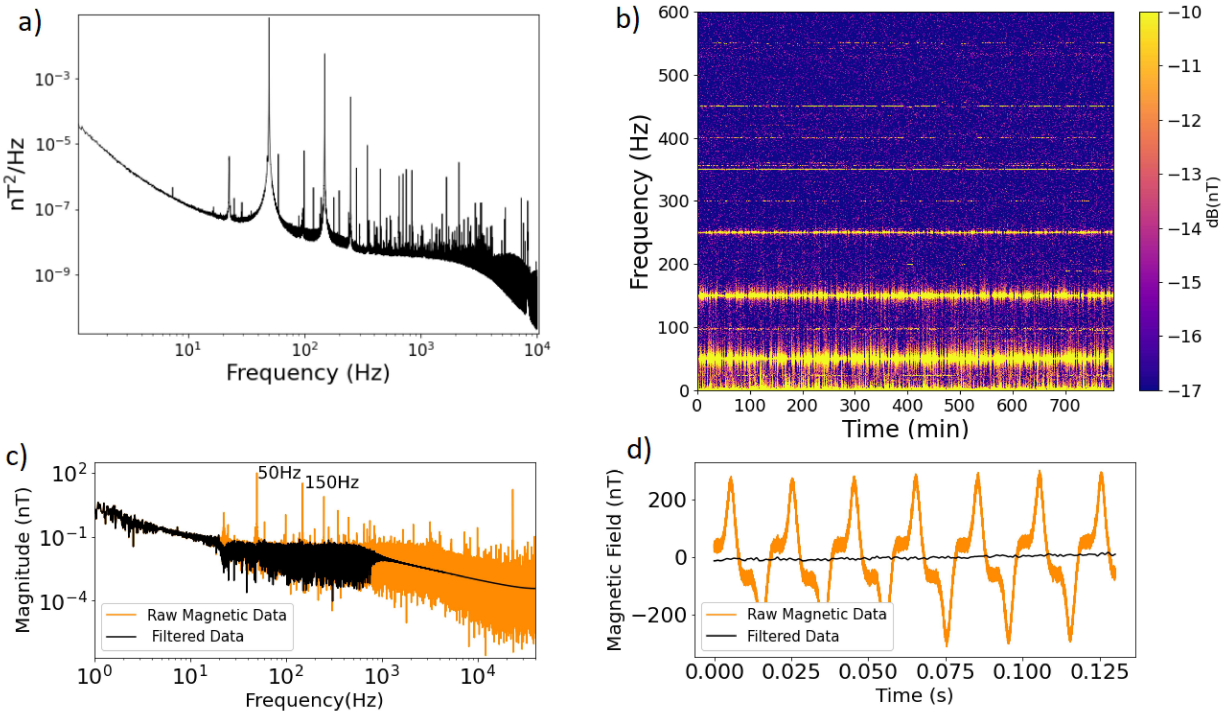

PLEASE CITE THIS ARTICLE AS DOI: 10.1116/5.0106099

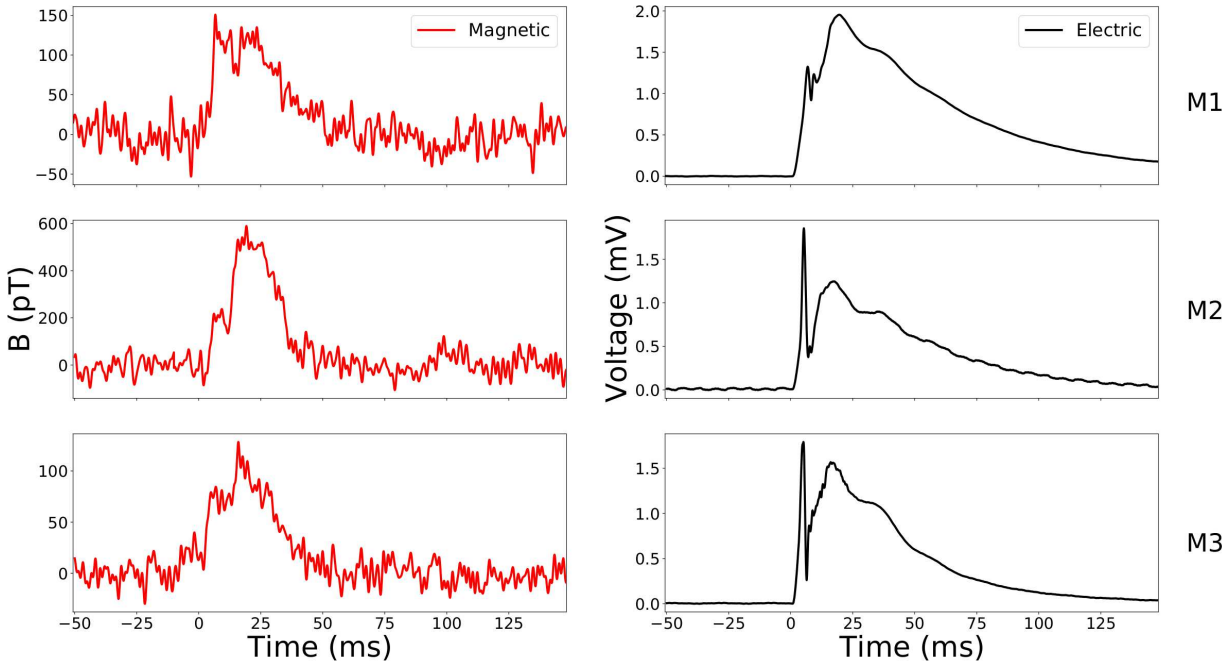

PLEASE CITE THIS ARTICLE AS DOI: 10.1116/5.0106099

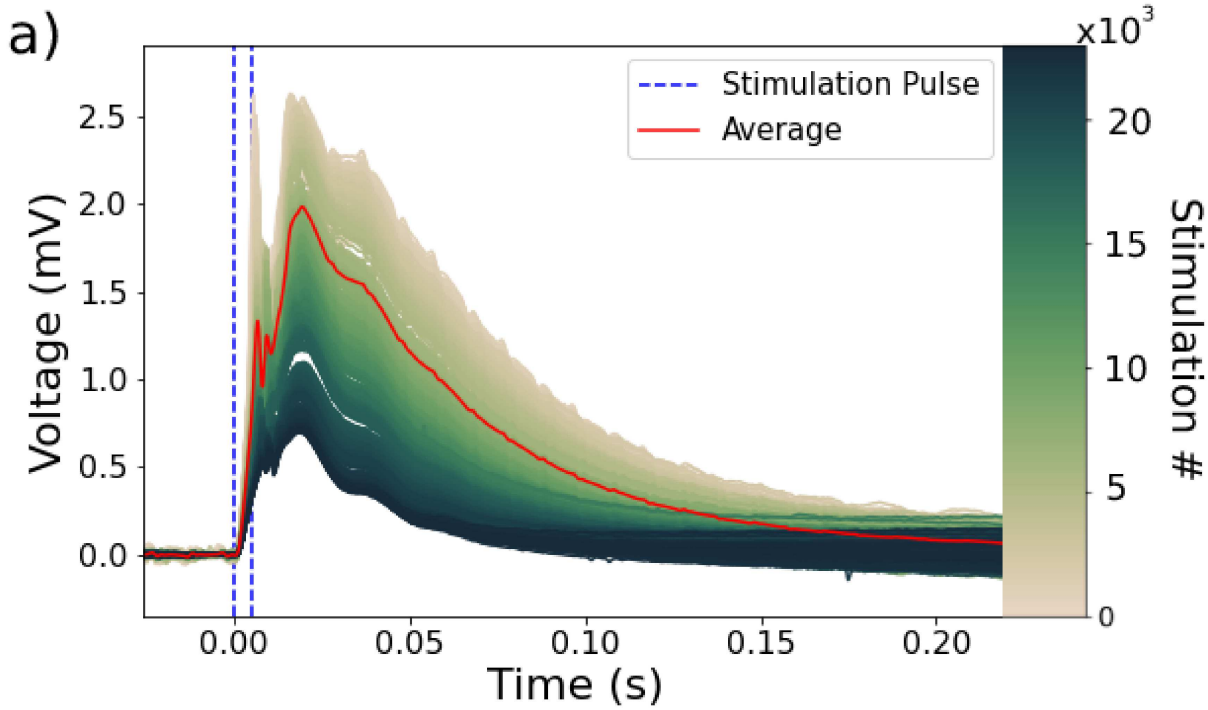

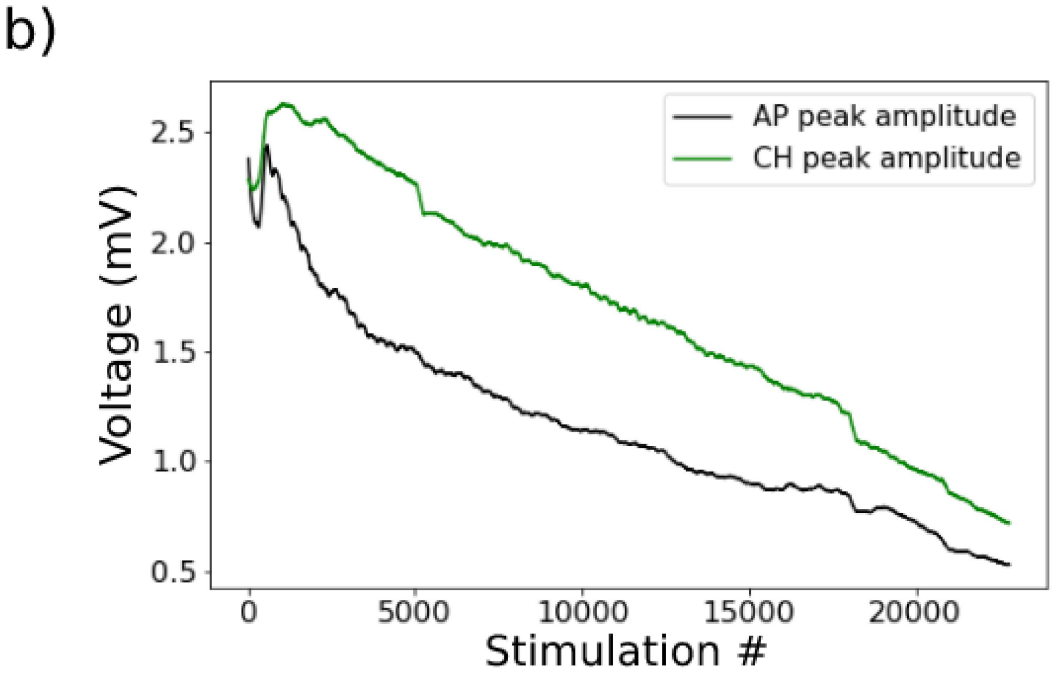

PLEASE CITE THIS ARTICLE AS DOI: 10.1116/5.0106099